Journal of Power Sources 260 (2014) 218–224

Contents lists available at ScienceDirect

Journal of Power Sources

journal homepage: www.elsevier.com/locate/jpowsour

Short communication

# Lithium storage mechanism in superior high capacity copper nitrate hydrate anode material

Xinxin Jiang, Kaiqiang Wu, Lianyi Shao, Miao Shui, Xiaoting Lin, Mengmeng Lao, Nengbing Long, Yuanlong Ren, Jie Shu*

*Faculty of Materials Science and Chemical Engineering, Ningbo University, Ningbo 315211, Zhejiang Province, People's Republic of China*

## HIGHLIGHTS

- Lithium storage process in $Cu(NO_3)_2 \cdot 2.5H_2O$ is studied by various *ex-situ* techniques.
- $Cu(NO_3)_2 \cdot 2.5H_2O$ reveals quasi-reversible conversion mechanism for lithium storage.
- $Cu(NO_3)_2 \cdot 2.5H_2O$ shows a lithium storage capacity of 2285.0 mAh $g^{-1}$.

## GRAPHICAL ABSTRACT

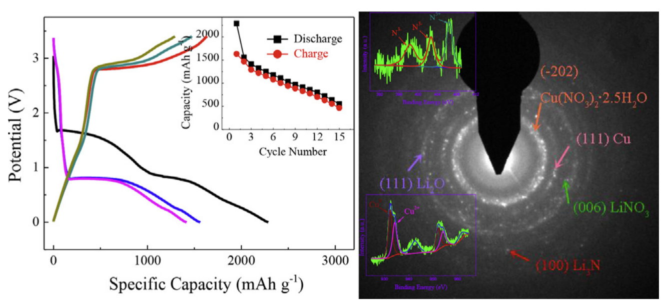


## ARTICLE INFO

*Article history:*
Received 30 December 2013
Received in revised form
6 February 2014
Accepted 6 March 2014
Available online 16 March 2014

*Keywords:*
Copper nitrate hydrate
Superior high capacity
Anode material
Lithium storage mechanism
Lithium-ion batteries

## ABSTRACT

Copper nitrate hydrate ($Cu(NO_3)_2 \cdot 2.5H_2O$) exhibits superior high lithium storage capacity (2285 mAh $g^{-1}$) as anode material for lithium-ion batteries. The structural transformation and lithium storage mechanism of $Cu(NO_3)_2 \cdot 2.5H_2O$ are thoroughly studied by various advanced analytical techniques. It is found that the lithium storage process of $Cu(NO_3)_2 \cdot 2.5H_2O$ is associated with a quasi-reversible electrochemical conversion reaction. During the discharge process, the electrochemical reaction of $Cu(NO_3)_2 \cdot 2.5H_2O$ with lithium results in the formation of Cu, $LiNO_3$, $Li_3N$, $Li_2O$ and $H_2O$. In the reverse charge process, $Cu(NO_3)_2$ can be generated by a conversion reaction. As a result, $Cu(NO_3)_2 \cdot 2.5H_2O$ shows the reversible charge capacities of 1632.1 mAh $g^{-1}$ in 0.0–3.4 V and 689.1 mAh $g^{-1}$ in 1.0–3.4 V, respectively.



## 1. Introduction

Recently, energy storage batteries for transportation and communication have gradually become the main power sources owing to global energy issues. Among these rechargeable energy storage batteries, lithium-ion batteries are dominant in the electric vehicles and portable electronics market for their advanced characteristics, such as high energy density and long cycling life [1–4]. However, anode materials have been focused on the carbonaceous materials, such as graphite [5,6], carbon nanotube [7,8], since the lithium-ion batteries were developed in 1991. Nowadays, these carbonaceous materials cannot satisfy the demands of the market. Therefore, intensive worldwide attempts have been done to develop novel high capacity materials to take place of carbonaceous materials in the past two decades.

According to the previous studies, Cu-based metal oxides and nitrides, such as CuO [9–11] and $Cu_3N$ [12], attract intensive

* Corresponding author. Tel.: +86 574 87600787; fax: +86 574 87609987.
*E-mail addresses:* shuimiao@nbu.edu.cn (M. Shui), shujie@nbu.edu.cn, sergio_shu@hotmail.com (J. Shu).

http://dx.doi.org/10.1016/j.jpowsour.2014.03.021
0378-7753/

attentions from researchers all over the world. CuO with high theoretical capacity (670 mAh $g^{-1}$), various structural patterns and inexpensive price has activated lots of attentions in recent years. $Cu_3N$, which exhibits high reversible capacity of 1280 mAh $g^{-1}$, good cycle life and excellent rate capability, is also examined as a candidate anode material for rechargeable lithium-ion batteries. Whether CuO, $Cu_3N$, $CuF_2$ or $CuCl_2$, their lithium storage mechanisms are based the reversible conversion reactions between $Li_xM$/Cu and Li/$Cu_yM_z$ (M = O, N, Cl, F) [9–14].

In most recent, copper nitrate hydrate ($Cu(NO_3)_2 \cdot xH_2O$) with high specific capacity has been investigated by our group as a novel anode material for lithium-ion batteries [15]. It is found that $Cu(NO_3)_2 \cdot xH_2O$ can deliver an initial discharge capacity higher than 2200 mAh $g^{-1}$. This superior high lithium storage capacity is much higher than all the ever reported transition metal oxides and nitrides, which generally show the initial discharge capacities of 1000–1500 mAh $g^{-1}$ as anode materials. After 30 cycles, a large reversible charge capacity of 597.6 mAh $g^{-1}$ can be maintained for $Cu(NO_3)_2 \cdot xH_2O$. As a result, $Cu(NO_3)_2 \cdot xH_2O$ shows outstanding potential as high capacity anode material for lithium-ion batteries. However, the structural transformation and lithium storage mechanism of high-capacity $Cu(NO_3)_2 \cdot xH_2O$ material during charge–discharge cycles were not investigated. To inspire the researchers to develop novel high capacity anode materials, it is necessary to discover the characteristics of superior high lithium storage capability.

In this paper, the structural transformation and lithium storage mechanism of high-capacity $Cu(NO_3)_2 \cdot 2.5H_2O$ materials are thoroughly studied by *ex-situ* X-ray photoelectron spectroscopy (XPS), *ex-situ* high-resolution transmission electron microscopy (HRTEM), *ex-situ* selected-area electron diffraction (SAED), *ex-situ* Fourier transform infrared spectroscopy (FTIR) techniques. A quasi-reversible conversion reaction mechanism between $Cu(NO_3)_2 \cdot 2.5H_2O$ with Li is discussed and proposed for the first time in this work.

## 2. Experimental

For being as active material, $Cu(NO_3)_2 \cdot 2.5H_2O$ powder (analytical grade, Aladdin Chemistry) was used as received and dried at 80 °C under vacuum before electrode preparation. The slurry for working electrode was composed of $Cu(NO_3)_2 \cdot 2.5H_2O$ powder as active material, carbon black as conductive additive, and polyvinylidene fluoride as a binder with a weight composition of 4:1:1 in N-methyl pyrrolidinone solvent. Then the slurry was coated on a Cu-foil current collector and dried at 80 °C under vacuum for 12 h. Discs with a diameter of 15 mm were cut and used as working electrodes.

The simulated $Cu(NO_3)_2 \cdot 2.5H_2O$/Li cells were assembled by using $Cu(NO_3)_2 \cdot 2.5H_2O$ disc as working electrode, metal lithium foil as counter electrode, Whatman glass fiber as separator and 1 mol $L^{-1}$ $LiPF_6$ dissolved in ethylene carbonate-dimethyl carbonate (1:1 in volume) as electrolyte. All the $Cu(NO_3)_2 \cdot 2.5H_2O$/Li cells were assembled in an argon-filled glove box at room temperature.

The charge–discharge cycles were measured by a constant-current density (50 mA $g^{-1}$) on multi-channel Land battery test system. X-ray diffraction (XRD) pattern of $Cu(NO_3)_2 \cdot 2.5H_2O$ was collected by a Bruker D8 Focus powder X-ray diffraction instrument with Cu Kα radiation. SEM image was achieved by a Hitachi S3400 scanning electron microscopy. XPS investigation was measured by a focused and monochromatized Al Kα radiation with a Kratos Axis Ultra spectrometer. The structural evolution of $Cu(NO_3)_2 \cdot 2.5H_2O$ during charge–discharge cycles was directly imaged by a JEOL JEM-

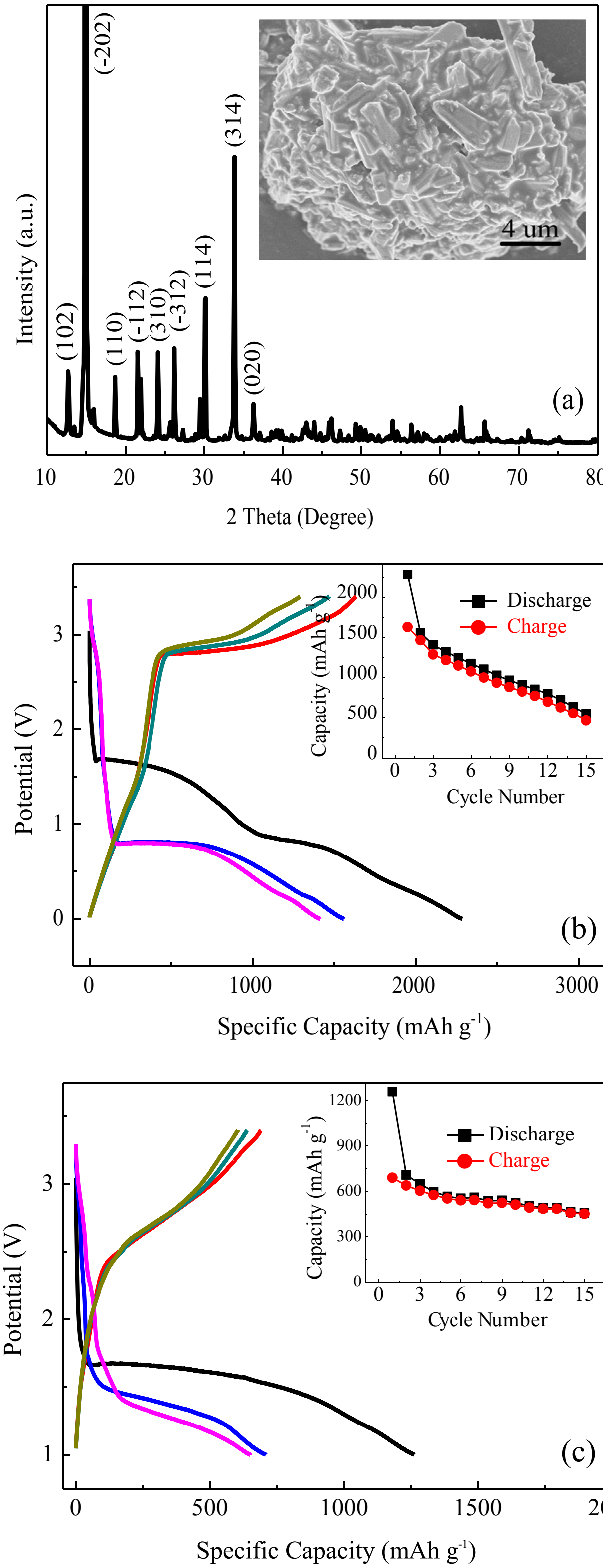


**Fig. 1.** (a) XRD pattern and corresponding SEM image of $Cu(NO_3)_2 \cdot 2.5H_2O$ powders, (b) charge–discharge curves and corresponding cyclic performance of $Cu(NO_3)_2 \cdot 2.5H_2O$ in 0.0–3.4 V and (c) charge–discharge curves and corresponding cyclic performance of $Cu(NO_3)_2 \cdot 2.5H_2O$ in 1.0–3.4 V.

2100 high-resolution transmission electron microscopy. The samples for SAED and HRTEM analysis were washed by dimethyl carbonate and vacuumed for 5 h before use.

## 3. Results and discussion

The XRD pattern and SEM image of $Cu(NO_3)_2\cdot 2.5H_2O$ powder are shown in Fig. 1(a). Seen from the XRD pattern, the nine strongest diffraction peaks located at 12.68°, 14.91°, 18.64°, 21.59°, 21.90°, 24.13°, 26.15°, 30.23° and 33.87° are well consistent with the (102), (-202), (110), (-112), (112), (310), (-312), (114) and (-602) lines of $Cu(NO_3)_2\cdot 2.5H_2O$ in JCPDS card No. 75-1493 (space group: I2/c), which shows the high-degree purity of active material for studying its structural evolutions during lithiation–delithiation process. The surface morphology for $Cu(NO_3)_2\cdot 2.5H_2O$ powder can be observed as the SEM image shown in Fig. 1(a). It is clear that $Cu(NO_3)_2\cdot 2.5H_2O$ particles with size of 2–4 μm aggregate into bigger secondary blocks with size of 20 μm.

Fig. 1(b) and (c) shows the first three charge–discharge cycles and corresponding cycle properties of $Cu(NO_3)_2\cdot 2.5H_2O$ electrodes at a current density of 50 mA $g^{-1}$ in 0.0–3.4 V and 1.0–3.4 V, respectively. Two potential plateaus at 1.68 and 0.85 V and one slope between 0.0 and 0.5 V can be observed in the initial discharge process as shown in Fig 1(b). This electrochemical behavior is quite different from that of CuO [9–11]. Based on the former research [13], it can be deduced that the lithiation plateau at 1.68 V is probable associated with the decomposition of $Cu(NO_3)_2\cdot 2.5H_2O$ into Cu, $H_2O$, $LiNO_3$ and/or $Li_3N$ and $Li_2O$, and the potential plateau at 0.85 V can be ascribed to the growth of solid electrolyte interphase film (SEI) [16,17], thus leading to the extra capacity and high irreversible capacity. The slope between 0.0 and 0.5 V is partially related to the formation of polymeric film [13,14]. Besides, this slope is also associated with the probable further decomposition of $LiNO_3$ into $Li_2O$ and $Li_3N$, which is similar to the electrochemical decomposition of $Li_2CO_3$ and LiOH during lithiation process [18–20] In the reverse charge process, only one long delithiation plateau at 2.82 V can be observed and it maintains the shape and potential in the following cycles. This high delithiation potential may be associated with formation of nitrate and the partial decomposition of polymeric and SEI films. During the second discharge process, one long and flat lithiation plateau appears at 0.80 V. Moreover, the slope between 0.0 and 0.8 V is kept. As a result, the discharge capacity decreases from 2285.0 to 1557.2 mAh $g^{-1}$. It suggests that the first lithiation–delithiation process is a partially reversible electrochemical reaction. In contrast, the charge capacity only reveals slight decrease from 1632.1 to 1468.8 mAh $g^{-1}$ in the initial two cycles. It indicates that the regenerated nitrate is an electrochemically active material. Upon long-term cycles, the charge capacity drops dramatically from 1632.1 to 467.4 mAh $g^{-1}$ in the initial 15 cycles in the working window of 0.0–3.4 V as shown in Fig. 1(b). The poor capacity retention is probably attributed to the repeated formation/decomposition of SEI and polymeric films. Through suppressing the effect of SEI and polymeric films with higher cutoff, the electrochemical behavior of $Cu(NO_3)_2\cdot 2.5H_2O$ is improved between 1.0 and 3.4 V as shown in Fig. 1(c). Although $Cu(NO_3)_2\cdot 2.5H_2O$ shows relative low initial discharge and charge capacities of 1260.4 and 689.1 mAh $g^{-1}$, the reversible discharge and charge capacities can be maintained at 456.9 and 451.4 mAh $g^{-1}$ after 15 cycles. This result demonstrates that high irreversible capacity loss and poor cyclic stability are mainly owing to the formation/decomposition of SEI and polymeric films during repeated cycles. Besides, the existence of $H_2O$ from irreversible decomposition of $Cu(NO_3)_2\cdot 2.5H_2O$ also has adverse effect on the capacity loss and cycling properties [21].

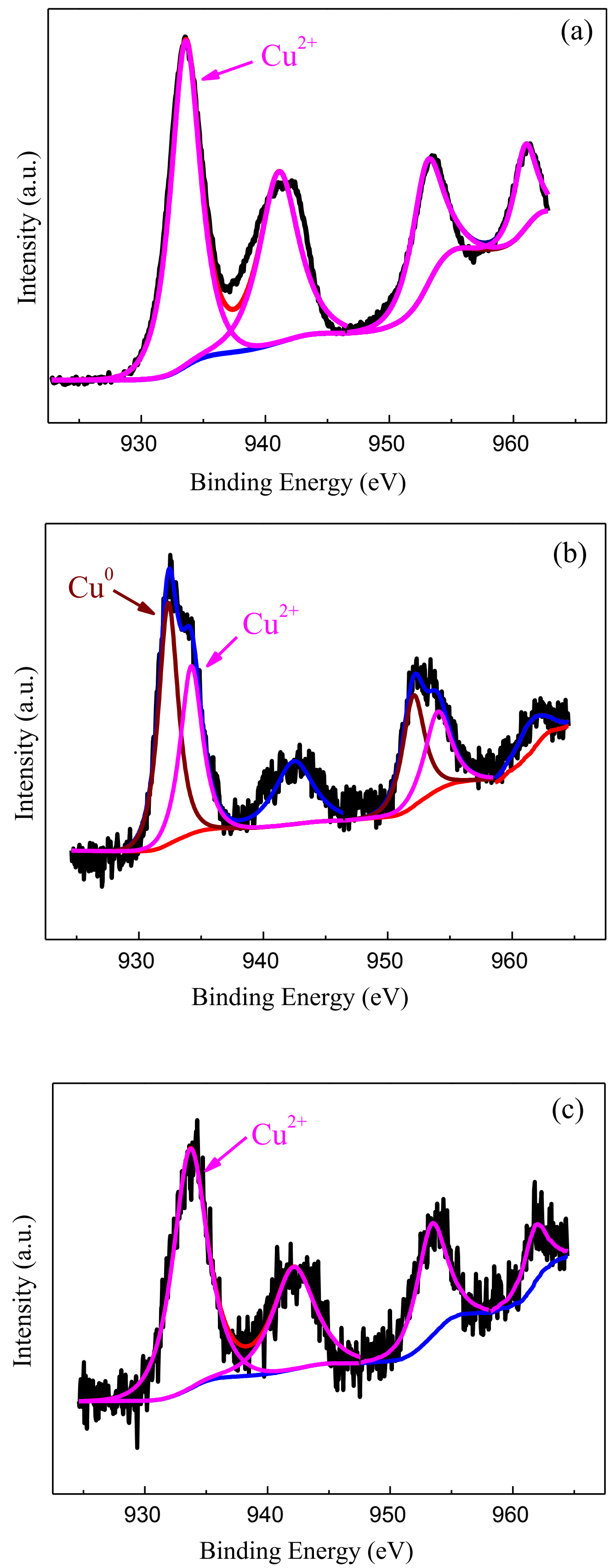


**Fig. 2.** XPS spectra of Cu element for $Cu(NO_3)_2\cdot 2.5H_2O$ sample with different lithiated and delithiated states. (a) The pristine sample, (b) discharged to 0.0 V and (c) charged to 3.4 V.

As a novel anode material, the investigation on the lithiation–delithiation mechanism of $Cu(NO_3)_2\cdot2.5H_2O$ is necessary for improving its electrochemical properties. Normally, the structural transformation of $Cu(NO_3)_2\cdot2.5H_2O$ electrode during charge–discharge cycle can be tested by various *ex-situ* methods. Here, the lithium storage mechanism of $Cu(NO_3)_2\cdot2.5H_2O$ in 0.0–3.4 V was investigated by *ex-situ* XPS, *ex-situ* FTIR, *ex-situ* HRTEM and *ex-situ* SAED techniques.

To avoid the effect of Cu, the powder working electrode for XPS observation is free of Cu current collector. It consists of $Cu(NO_3)_2\cdot2.5H_2O$ and carbon black with a weight ratio of 4:1. To keep the structure of electrode, the samples are directly used for analysis without washing by dimethyl carbonate. The XPS spectra of Cu and N elements in different lithiated and delithiated states during the first cycle are shown in Figs. 2 and 3, respectively. Fig. 3(a) displays the feactured $Cu^{2+}$ ($2p_{3/2}$) and $Cu^{2+}$ ($2p_{1/2}$) peaks from pristine sample at 933.5 and 953.5 eV, respectively, based on the Handbook of X-Ray Photoelectron Spectroscopy [22]. Moreover, two satellite peaks for $Cu^{2+}$ can be observed at 941.0 and 961.1 eV. The N 1s peak ($N^{5+}$) at 407.2 eV in Fig. 3(a) can be attributed to $NO_3^-$ group in $Cu(NO_3)_2\cdot2.5H_2O$ [23].

After a discharge process to 0.0 V, $Cu^0$ ($2p_{3/2}$) and $Cu^0$ ($2p_{1/2}$) can be respectively detected at 932.3 and 952.1 eV as shown in Fig. 2(b) [22]. That shows the transformation from $Cu^{2+}$ to $Cu^0$ during the first discharge process. However, $Cu^{2+}$ featured peaks (934.0 and 954.1 eV) can still be observed, which is due to some unreacted active materials existing in this special Cu-foil free thick powder electrode (35 mg) for XPS observation. Furthermore, massive changes can be observed with the N element after a discharge process to 0.0 V as shown in Fig. 3(b). The $N^{5+}$ in $NO_3^-$ group was partially converted into $N^{3-}$ for the appearance of the feactured peaks at 398.2 and 402.7 eV, indicating the generation of $Li_3N$ [22]. Besides, a slight change for $N^{5+}$ from 407.2 to 406.5 eV during the first discharge process, indicating the conversion generation of $LiNO_3$ from $Cu(NO_3)_2\cdot2.5H_2O$. The formation of lithiated products is also confirmed by the appearance of Li 1s peak at 54.9 eV as shown in Fig. S1 (Supplementary Materials). No characteristic peaks of $NO_2^-$ group can be detected in Fig. 2(b), suggesting the impossible appearance of the reduction transformation from $NO_3^-$ to $NO_2^-$ during the first discharge process.

With a reverse charge to 3.4 V, $Cu^0$ peaks totally disappear and $Cu^{2+}$ peaks become strong again, indicating $Cu^0$ absolutely transforms into $Cu^{2+}$ in the delithiation process as shown in Fig. 2(c). In the charging process, the featured peak of $N^{3-}$ at 402.8 eV in Fig. 3(c) becomes weak but does not disappear, and the $N^{5+}$ peak (407.2 eV) in $NO_3^-$ become strong again, indicating the partial decomposition of $Li_3N$ and the regeneration of $NO_3^-$. This phenomenon is in accordance with the observed result of *ex-situ* FTIR analysis as shown in Fig. S3 (Supplementary Materials). It shows the existence of $NO_3^-$ group and its partially reversible intensity change during charge–discharge process. It also suggests that the electrochemical reaction between $Cu(NO_3)_2\cdot2.5H_2O$ with Li is a partially reversible process.

In order to further confirm the lithiated and delithiated products, *ex-situ* SAED and HRTEM techniques were used to identify the phases generated during discharge–charge process. The test results of *ex-situ* SAED and HRTEM observation for lithiated $Cu(NO_3)_2\cdot2.5H_2O$ sample can be observed in Fig. 4. As the HRTEM images depicted in Fig. 4(a) and (b), lithiated $Cu(NO_3)_2\cdot2.5H_2O$ sample shows the random orientation of nanocrystals enwrapped by amorphous carbon black. It can be clearly observed that many small ordered domains are dispersed in the carbon matrix. The characteristic distances of ordered domains are 5.930, 3.182, 2.120 and 3.630 Å in Fig. 4(a) which are close to the interplanar distances of (-202), (100), (111) and (012) planes, representing

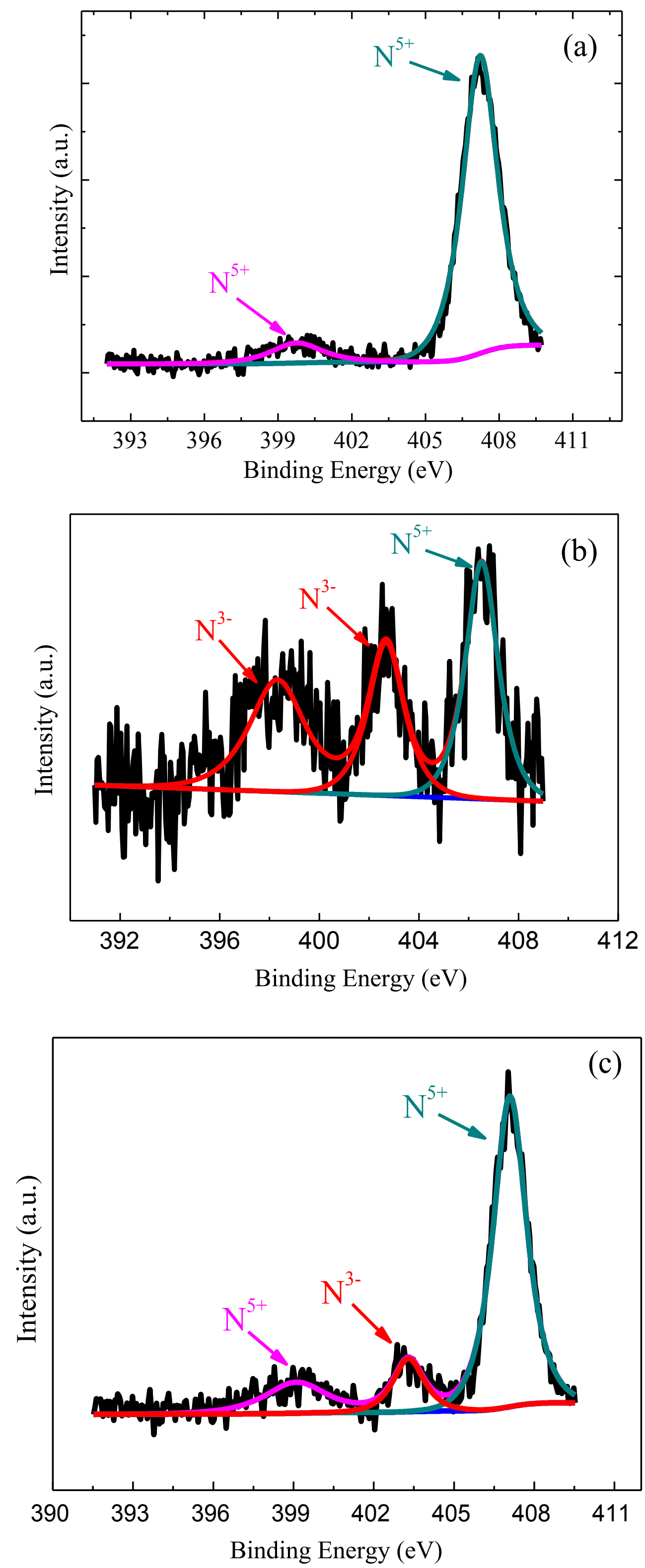


**Fig. 3.** XPS spectra of N element for $Cu(NO_3)_2\cdot2.5H_2O$ sample with different lithiated and delithiated states. (a) The pristine sample, (b) discharged to 0.0 V and (c) charged to 3.4 V.

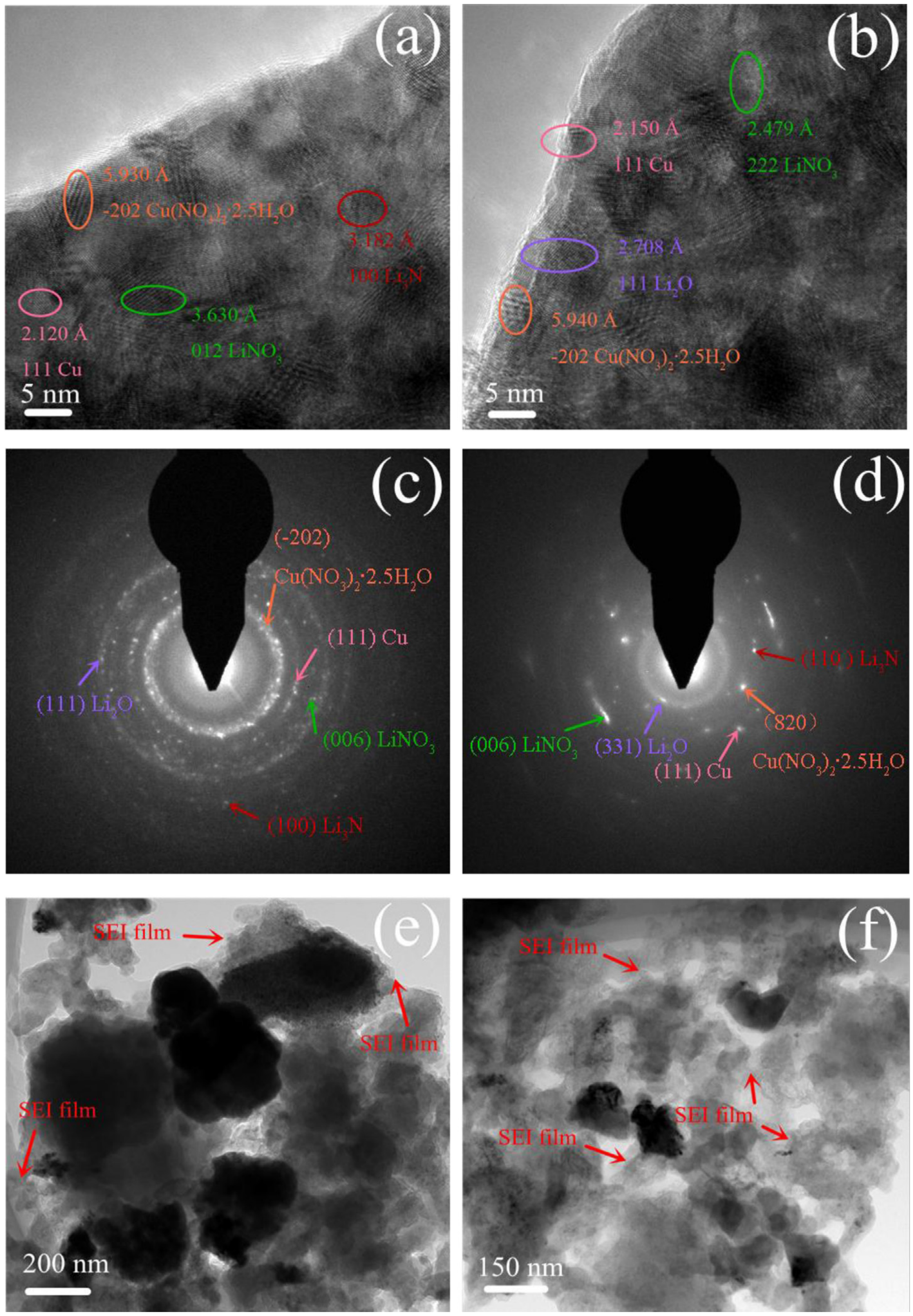


**Fig. 4.** (a, b) HRTEM images, (c, d) corresponding SAED patterns and (e, f) low-resolution TEM patterns of lithiated $Cu(NO_3)_2 \cdot 2.5H_2O$ sample after a discharge process to 0.0 V.

$Cu(NO_3)_2 \cdot 2.5H_2O$ (JCPDS card No. 75-1493), $Li_3N$ (JCPDS card No. 76-0822), Cu (JCPDS card No. 85-1326) and $LiNO_3$ (JCPDS card No. 08-0466), respectively. Moreover, different ordered domains can be observed by HRTEM as shown in Fig. 4(b). The distances between two lattice fringes in four different regions are 2.479, 2.150, 2.708 and 5.940 Å corresponding to the (006) plane of $LiNO_3$, (111) plane of Cu, (111) plane of $Li_2O$ (JCPDS card No. 77-2144) and (-202) plane of $Cu(NO_3)_2 \cdot 2.5H_2O$. The SAED pattern of the lithiated electrode in Fig. 4(c) reveals a series of rings with corresponding interplanar distances of 1.552, 2.047, 2.453, 2.749 and 3.268 Å which can respectively be assigned to the (028) plane of $Cu(NO_3)_2 \cdot 2.5H_2O$, (111) plane of Cu, (006) plane of $LiNO_3$, (111) plane of $Li_2O$ and (100) plane of $Li_3N$. Fig. 4(d) also shows another reflections of SAED pattern, in which the interplanar distances are 1.084, 1.567, 1.777, 2.137 and 2.488 Å corresponding to the (331) plane of $Li_2O$, (820) plane of $Cu(NO_3)_2 \cdot 2.5H_2O$, (110) plane of $Li_3N$, (111) plane of Cu and (006) plane of $LiNO_3$. Here, the identification of $Li_3N$, Cu, $LiNO_3$ and $Li_2O$ in HRTEM and SAED observation is in accordance with the analytical result of XPS technique. The existence of $Cu(NO_3)_2 \cdot 2.5H_2O$ during HRTEM and SAED observation is contributed to some unreacted particles in the huge powder electrode used in the experiment during the charge–discharge cycles. Besides, the appearance of amorphous film in Fig. 4(e) and (f) is associated to the formation of thick polymeric and SEI films [13,14].

Fig. 5 shows the HRTEM and SEAD images of delithiated $Cu(NO_3)_2 \cdot 2.5H_2O$ sample after a reverse charge to 3.4 V. It can be

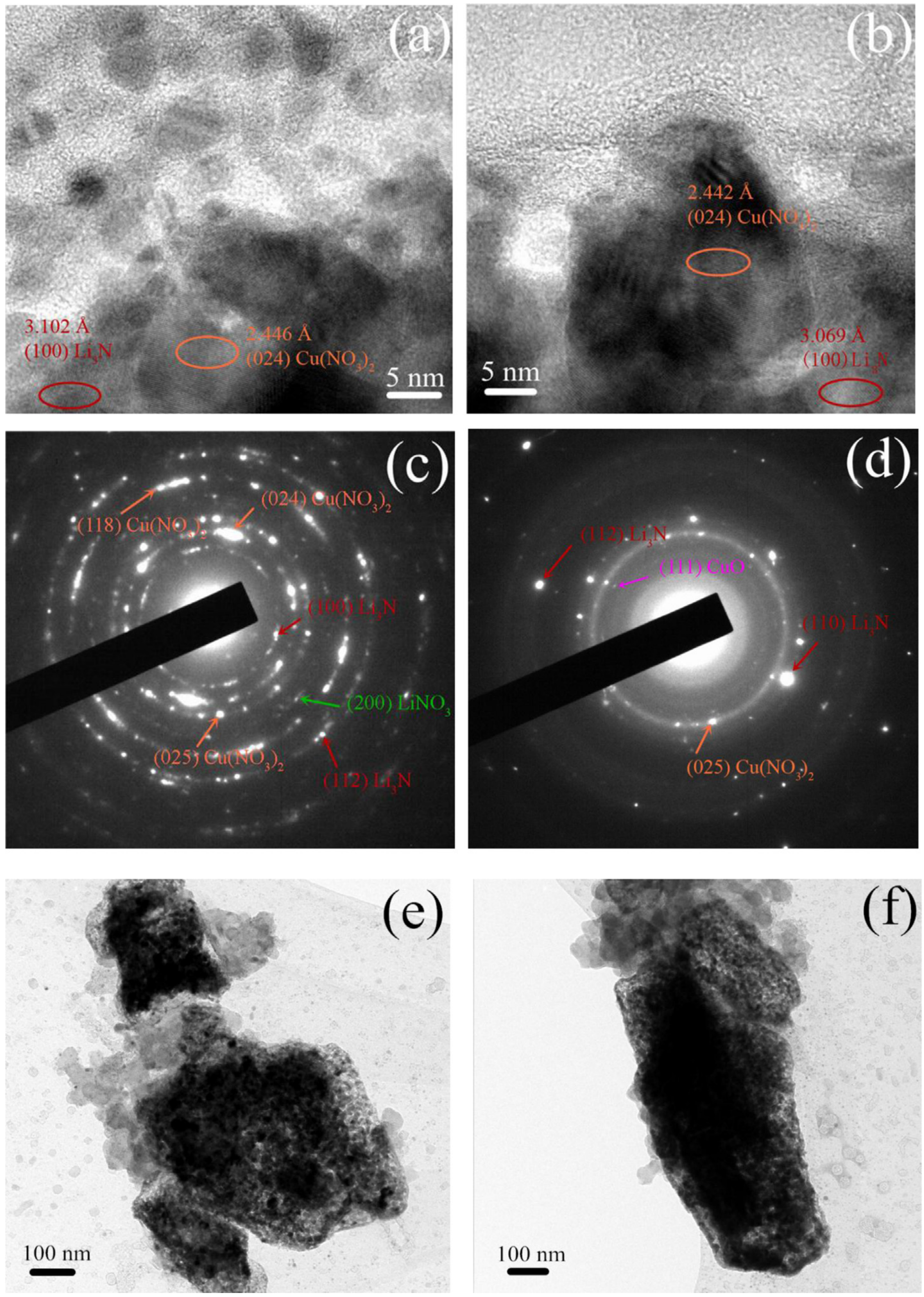


**Fig. 5.** (a, b) HRTEM images, (c, d) corresponding SAED patterns and (e, f) low-resolution TEM patterns of delithiated $Cu(NO_3)_2 \cdot 2.5H_2O$ sample after a charge process to 3.4 V.

clearly observed that only two kinds of interplanar distances (3.102 and 2.446 Å) are detected in Fig. 5(a), which are respectively ascribed to the (100) plane of $Li_3N$ and (024) plane of $Cu(NO_3)_2$ (JCPDS card No. 87-1663). Same interplanar distances can be observed in Fig. 5(b) which are consistent with the results of XPS analysis in Figs. 3 and 4, showing only $Cu^{2+}$ is detected for Cu element and partial $N^{3-}$ still exist after initial charge process. Besides, $LiNO_3$ and CuO also can be observed in Fig. 5(c) and (d), corresponding to two ring patterns of the (200) plane of $LiNO_3$ and (111) plane of CuO (JCPDS card No. 80-1917). This result confirms that some $LiNO_3$ lose their electrochemical activity and remain in the electrode during the delithiation process. Furthermore, the feactured ring for CuO is very weak, indicating trace $Li_2O$ and Cu transform into CuO during the delithiation process. Viewed from Fig. 5(c) and (d), other ring patterns can be contributed to the (118), (024) and (025) planes of $Cu(NO_3)_2$, (100) and (112) planes of $Li_3N$, (025) plane of $Cu(NO_3)_2$, (112) and (110) planes of $Li_3N$. It suggests that the lithiated products can be quasi-reversibly converted into $Cu(NO_3)_2$ after a charge process to 3.4 V. As a result, regenerated secondary particles can be observed in Fig. 5(e) and (f). $Cu(NO_3)_2$ reveals a long and flat lithiation plateau at 0.80 V, which is quite different from the electrochemical behavior of $Cu_3N$ [12], CuO [9–11,24,25] and $Cu_2O$ [26,27]. Notably, an unknown ring pattern (about 2.736 Å) is also detected in Fig. 5(d) that may be the featured interplanar distance of copper nitrides, such as $Cu_3N_2$. As the above analysis, the main structural evolution of $Cu(NO_3)_2 \cdot 2.5H_2O$ for the first lithiation and delithiation process can be expressed as follows:

$$Cu(NO_3)_2 \cdot 2.5H_2O + (18-8x)Li^+ + (18-8x)e^- \xrightarrow{\text{Disharge}} Cu + xLiNO_3 + (2-x)Li_3N + (6-3x)Li_2O + 2.5H_2O \quad (1)$$

$$yLi^+ + ye^- + \text{electrolyte} \xrightarrow{\text{Discharge}} SEI \quad (2)$$

$$Cu + xLiNO_3 + (2-x)Li_3N + (6-3x)Li_2O \xrightarrow{\text{Charge}} Cu(NO_3)_2 + (18-8x)Li^+ + (18-8x)e^- \quad (3)$$

Besides, the appearance of weak CuO ring and unknown pattern in Fig. 5(d) suggests the probable formation of copper oxides and nitrides during the charge process. However, the disappearance of characteristic electrochemical behaviors of copper oxides and nitrides in Fig. 1 indicates that most $Cu^0$ transform into $Cu(NO_3)_2$ and trace $Cu^0$ may be ascribed to the generation of CuO and $Cu_3N_2$ during the charge process.

$$Li_2O + Cu \xrightarrow{\text{Charge}} CuO + 2Li^+ + 2e^- \quad (4)$$

$$2Li_3N + 3Cu \xrightarrow{\text{Charge}} Cu_3N_2 + 6Li^+ + 6e^- \quad (5)$$

## 4. Conclusions

In this paper, the structural transformation of $Cu(NO_3)_2 \cdot 2.5H_2O$ anode material was studied by *ex-situ* XPS, FTIR, HRTEM and SAED techniques. A probable lithiation–delithiation mechanism of $Cu(NO_3)_2 \cdot 2.5H_2O$ is proposed according to the observations. The investigation results show that the generation of Cu, $Li_3N$, $LiNO_3$ and $Li_2O$ after discharge to 0.0 V is contributed to the lithiation plateaus and slopes in the first discharge process. The long delithiation plateau at 2.82 V in the first charge process is mainly assigned to the generation of $Cu(NO_3)_2$. Moreover, trace other Cu-based compounds, such as CuO and $Cu_3N_2$, can be observed indicating partial $Li_2O$ and $Li_3N$ transform into CuO and $Cu_3N_2$ after a reverse charge to 3.4 V. Thus, quasi-reversible conversion reaction between $Cu(NO_3)_2 \cdot 2.5H_2O$ and Li is responsible for the superior high lithium storage capacity of 2285.0 mAh $g^{-1}$ and lithium release capacity of 1632.1 mAh $g^{-1}$.

## Acknowledgments

This work is sponsored by National Natural Science Foundation of China (No. 51104092) and National 863 Program (2013AA050901). The work is also supported by K.C. Wong Magna Fund in Ningbo University.

## Appendix A. Supplementary data

Supplementary data related to this article can be found at http://dx.doi.org/10.1016/j.jpowsour.2014.03.021.

## References

[1] M. Armand, J.M. Tarascon, Nature 451 (2008) 652–657.
[2] J. Hassoun, P. Reale, S. Panero, B. Scrosati, M. Wachtler, M. Fleischhammer, M. Kasper, M.W. Mehrens, Electrochim. Acta 55 (2010) 4194–4200.
[3] J.S. Chen, Y.L. Tan, C.M. Li, Y.L. Cheah, D.Y. Luan, S. Madhavi, F.Y.C. Boey, L.A. Archer, X.W. Lou, J. Am. Chem. Soc. 132 (2010) 6124–6130.
[4] B.B. Tian, H.F. Xiang, L. Zheng, Z. Li, H.H. Wang, Electrochim. Acta 55 (2010) 5453–5458.
[5] Y. Qi, S.J. Harris, J. Electrochem. Soc. 157 (2010) 741–747.
[6] F. Croce, G.B. Appetecchi, L. Persi, B. Scrosati, Nature 394 (1998) 456–458.
[7] C.D.L. Casas, W.Z. Li, J. Power Sources 208 (2012) 74–85.
[8] D.S. Su, R. Schlogl, ChemSusChem 3 (2010) 136–168.
[9] J.Y. Xiang, J.P. Tu, X.H. Huang, Y.F. Yuan, X.L. Wang, X.H. Huang, Z.Y. Zeng, Electrochim. Acta 54 (2009) 1160–1165.
[10] S.Q. Wang, J.Y. Zhang, C.H. Chen, Scr. Mater. 57 (2007) 337–340.
[11] M. Yang, Q.M. Gao, Micropor. Mesopor. Mater. 143 (2011) 230–235.
[12] N. Pereira, L. Dupont, J.M. Tarascon, L.C. Klein, G.G. Amatucci, J. Electrochem. Soc. 150 (2003) A1270–A1280.
[13] S. Laruelle, S. Grugeon, P. Poizot, M. Dolle, L. Dupont, J.-M. Tarascon, J. Electrochem. Soc. 149 (2002) A627–A634.
[14] A. Debart, L. Dupont, P. Poizot, J.-B. Leriche, J.M. Tarascon, J. Electrochem. Soc. 148 (2001) A1266–A1274.
[15] K.Q. Wu, D.J. Wang, L.Y. Shao, M. Shui, R. Ma, M.M. Lao, N.B. Long, Y.L. Ren, J. Shu, J. Power Sources 248 (2014) 205–211.
[16] L. Martin, H. Martinez, D. Poinot, B. Pecquenard, F.L. Cras, J. Power Sources 248 (2014) 861–873.
[17] S.P. Kim, A.C.T. van Duin, V.B. Shenoy, J. Power Sources 196 (2011) 8590–8597.
[18] L.Y. Shao, R. Ma, K.Q. Wu, M. Shui, M.M. Lao, D.J. Wang, N.B. Long, Y.L. Ren, J. Shu, J. Alloys Compd. 581 (2013) 602–609.
[19] Y.Y. Hu, Z.G. Liu, K.W. Nam, O.J. Borkiewicz, J. Cheng, X. Hua, M.T. Dunstan, X.Q. Yu, K.M. Wiaderek, L.S. Du, K.W. Chapman, P.J. Chupas, X.Q. Yang, C.P. Grey, Nat. Mater. 12 (2013) 1130–1136.
[20] L.W. Su, Z. Zhou, X. Qin, Q.W. Tang, D.H. Wu, P.W. Shen, Nano Energy 2 (2013) 276–282.
[21] F. Joho, B. Rykart, R. Imhof, P. Novak, M.E. Spahr, A. Monnier, J. Power Sources 81-82 (1999) 243–247.
[22] J.F. Moulder, W.F. Stickle, P.E. Sobol, K.D. Bomben, Handbook of X-ray Photoelectron Spectroscopy, Perkin-Elmer, Minnesota, USA, 1993.
[23] J. Swialowska, V. Lair, C.P. Nabais, G. Cota, P. Marcus, A. Chagnes, Appl. Surf. Sci. 257 (2011) 9110–9119.
[24] J.Y. Xiang, J.P. Tu, L. Zhang, Y. Zhou, X.L. Wang, S.J. Shi, J. Power Sources 195 (2010) 313–319.
[25] F.S. Ke, L. Huang, G.Z. Wei, L.J. Xue, J.T. Li, B. Zhang, S.R. Chen, X.Y. Fan, S.G. Sun, Electrochim. Acta 54 (2009) 5825–5829.
[26] S.B. Ni, X.H. Lv, T. Li, X.L. Yang, L.L. Zhang, Electrochim. Acta 109 (2013) 419–425.
[27] X.Y. Shen, S. Chen, D.B. Mu, B.R. Wu, F. Wu, J. Power Sources 238 (2013) 173–179.